ACS Sustainable Chemistry & Engineering

pubs.acs.org/journal/ascecg

Research Article

Coated Magnetite Nanoparticles and *Tillandsia usneoides*: More Friends Than Foes

Veronica Butelli, Sara Falsini,* Alessio Papini, Maria Cristina Salvatici, Delphine Talbot, Ali Abou-Hassan, Cristina Gonnelli, and Sandra Ristori

Cite This: https://doi.org/10.1021/acssuschemeng.6c01219

Read Online

ACCESS | Metrics & More | Article Recommendations | Supporting Information

ABSTRACT: Micronutrient delivery by nanotechnology is becoming an effective strategy in plant fortification and growth. Among element deficiencies, one of the most detrimental is Fe ion shortage, in that it may affect many physiological processes, including photosynthetic and respiratory pathways. Here, we used citrate-stabilized magnetite nanoparticles (FeCi) which were postengineered by coverage with polysaccharides of natural origin, to produce biocompatible iron carriers. Specifically, *Aloe vera* extracts (APS) and exopolysaccharides from *Cyanospira capsulata* (EPS) were chosen as capping agents for magnetite nanoparticles to facilitate the interaction with the model plant *Tillandsia usneoides*. The complex structure of these novel nanohybrids was elucidated by in-depth physicochemical characterization. In the plant specimens, treatment with FeCi complexed with APS by foliar spray improved the growth and photosynthetic activity. This was attributed to a 3−4 times increase in iron content. In turn, this evidenced a synergistic activity between the nanoparticles and the employed polysaccharides. These results open the way to new agricultural applications that may contribute to ameliorating both the yield and quality of crops.

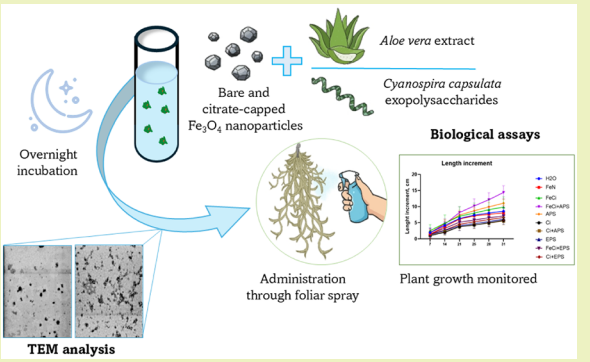

KEYWORDS: *magnetite nanoparticles, polysaccharides, nanohybrids, Tillandsia usneoides, Cyanospira capsulata, Aloe vera*

INTRODUCTION

Nanotechnology has recently been applied to plant science with positive outcomes,[1−3] fostering the development of new pesticides and fertilizers. Respect to their macroscopic counterparts, nanosystems show favorable properties such as sustained release and targeted delivery. In turn, the improved assimilation by plant tissues, granted by the small size of nanoformulations, allows us to use reduced amounts of agrochemicals, with beneficial effects for operators and the environment. Thus, it is now recognized that nanotechnology, especially if applied with biocompatible particles,[4−7] can be as valuable and more eco-friendly than genetic modification, which presents non-negligible societal challenges, despite its high technical potential.[8,9] Alike other innovative practices, nanotechnology aims to increase both the harvest yield and the crop quality to combat the so-called "hidden hunger", defined by FAO (www.fao.org) as deficiencies in micronutrients. Around two billion people currently suffer from hidden hunger, with women and children being particularly susceptible to these deficiencies.[10] Micronutrients also play a crucial role in plant productivity.[11,12] The main symptoms of their deficiency in plants include abnormal pigmentation and impairment of photosynthetic activity. The strong reliance of intensive agriculture on fertilizers, based on macronutrients (nitrogen, phosphorus, and potassium), has been identified as a factor of micronutrient depletion in soils and reduced micronutrient availability.[11] One of the most common deficient elements in soil is iron, and this can be a severe limitation for plant growth since the Fe(II)−Fe(III) redox switch takes an active part not only in the electron transport chain of photosynthesis and respiration, but also as a cofactor of numerous enzymes.[13]

Nanofertilizers represent an economically accessible and environmentally sustainable strategy for enhancing micronutrient availability by crops[14] and in this context nanoparticles made by metal or metal oxides are recognized as a potent means to deliver essential elements for vital processes in plants.[1,3] Two main routes can be followed for nanoparticle administration to plants: (i) spraying directly onto the plant surface is particularly effective for delivering nutrients and pesticides to the aerial parts, since it allows rapid absorption through stomata;[15] (ii) root administration, which entails applying nanoparticles to the soil, from where they are

Received: January 29, 2026
Revised: March 25, 2026
Accepted: March 31, 2026

absorbed and transported via the xylem. This latter approach is suitable for systemic delivery, but may cause unwanted accumulation of agrochemicals in the soil.[16,17]

Building on decades of applications to materials science and medicine, metal-based nanoparticles can be currently engineered to possess tailored physicochemical properties such as size, shape, surface charge, and surface functionalization, which are known to govern solubility in aqueous environments, redox activity, and interaction with plant cells. So, functionalization is a key aspect for the application of nanoparticles to plants, especially in light of recent studies which acknowledge that the cell wall, far from merely representing a passive barrier, plays a major role in cellular trafficking.[18] Another important aspect of surface capping with biocompatible agents is to reduce the possible toxicity of bare metal-based nanoparticles.[19−21]

Here we used magnetite (Fe_3O_4) nanoparticles stabilized by sodium citrate at the stage of synthesis as a vector of Fe ions. The same particles have already shown good performance in biomedical applications, i.e., photothermal therapy and ferroptosis.[22,23] Citrate-capped Fe_3O_4 nanoparticles were modified by further coverage with polysaccharides to obtain nanocomposites that can facilitate the interaction with the plant cell walls by similarity. Indeed, the chemical recognition among sugar units is a well-documented mechanism of interaction in biological systems and has been used to design receptors in cellular imaging as well as in therapeutics.[24,25] Moreover, being intended for a large-scale use, the present nanocomposites were prepared by choosing polysaccharides of natural origin, available in huge quantities and low cost, that is an added value from the point of view of circular economy.[26] Specifically, polymers from *Aloe vera* and *Cyanospira capsulata* were used to engineer the surface of citrate-stabilized magnetite nanoparticles. *Aloe vera* (L.) Burm.f. (syn. of *Aloe barbadensis* Miller, Asphodelaceae) is a succulent plant typical of hot and dry climates whose leaves can store a large amount of water due to their abundant parenchyma, a semisolid clear gel characterized by the presence of polysaccharides.[27,28] Aloe gel and extracts are known for their therapeutic and cosmetic properties and are also increasingly used as edible coatings for fruits and vegetables.[29] Moreover, several studies reported how *A. vera* extracts can be used as natural biostimulants, enhancing plant growth and modulating the production of bioactive compounds.[30−34] *Cyanospira capsulata* Florenzano, Sili, Pelosi, and Vincenzini is a species of cyanobacteria[35,36] possessing a gelatinous envelope composed by polysaccharides.[37] The choice of this polysaccharide source[38] was motivated by the fact that many studies have evidenced how microalgae can stimulate plant growth, productivity, and secondary metabolites synthesis.[39,40]

The obtained formulations were applied to *Tillandsia usneoides* (L.) L. (Bromeliaceae), commonly known as Spanish moss, an epiphytic plant of the Bromeliaceae family, which has been used as an air-quality biosensor,[41,42] since it can take up nutrients exclusively from the atmosphere through its numerous absorbing trichomes.[43,44] This characteristic and the absence of roots make *Tillandsia usneoides* a perfect candidate to test the foliar administration of nanosystems.

The main purpose of this work was devising novel delivery agents for Fe ions, which are vital nutrients for healthy plant growth. It was conducted first by characterizing the physicochemical properties of newly prepared nanohybrids and then by evaluating their potential to improve plant development. The ion dose for administration experiments was chosen in the range used in previous studies,[21,45] which described the toxic action of airborne magnetite nanoparticles (foes). This was done not only for the sake of comparison but also to explore the possibility of different effects entailed by Fe_3O_4 nanoparticles when engineered by appropriate coating (friends). The results obtained are very promising and encourage further studies in the direction of applying metal-based nanoparticles to suppress toxicity while improving delivery performance.

MATERIALS AND METHODS

Materials

Sodium hydroxide (NaOH, 98%), Fe^{2+} chloride tetrahydrate ($FeCl_2 \cdot 4H_2O$, 98%), and Fe^{3+} chloride hexahydrate ($FeCl_3 \cdot 6H_2O$, >97%) were obtained from Alfa Aesar. Trisodium citrate and nitric acid (HNO_3, 70%) were obtained from VWR (Paris, France). Ethyl acetate (>99.5%), acetone (technical grade), ethanol (96%), and diethyl ether (100%) were obtained from Sigma-Aldrich (Saint Quentin Fallavier, France).

For the synthesis of bare magnetite (FeN), a stoichiometric mixture of Fe^{2+} and Fe^{3+} chloride salts was mixed in a molar ratio of 1:2. The pH of the solution was increased to 10 by the addition of sodium hydroxide to induce precipitation and the formation of magnetite nanoparticles. The nanoparticles were isolated magnetically, washed with ethanol, ethyl acetate, then ethanol (three times each), before resuspending them finally in water at pH = 4. Citrate-stabilized (FeCi) colloidal suspensions were elaborated as described in our previous work.[23]

Bare and citrate-stabilized iron oxide nanoparticles were diluted with distilled water at pH 8 to obtain a stock solution at iron concentration of 1.25 mg/mL. This pH value was maintained throughout all the operations in the present work, since it is well compatible with both magnetite nanoparticles and plants, ensuring colloidal stability. FeCi nanoparticles were used as a starting material for further coating with two different polysaccharides, henceforth called APS and EPS, according to the procedure described below. The first polysaccharide was a gel obtained from a commercial product (Equilibra Aloe Detox Zero, Aloe Vera Gel Concentrato 99%), while the latter polysaccharide was extracted from *C. capsulata* cultured at the Department of Agriculture, Food, Environment and Forestry (DAGRI) of the University of Florence following the protocol of Vincenzini et al. (1990).[46] The APS gel was kept at 40 °C to obtain a dry material from which solutions at known concentration by weight could be obtained. Subsequently, both APS and EPS were dissolved in distilled water adjusted to pH 8 with KOH at the concentration of 2.5 mg/mL. These solutions were finally filtered with 0.45 and 0.20 μm Minisart carbon syringe filters (Sartorius s.r.l., Göttingen, Germany). A citrate (Ci) solution was also prepared in water at pH 8 in accordance with the concentration of citric acid present in the FeCi system for comparison purposes (0.025 mg/mL). All the analyses and applications to *Tillandsia usneoides* were carried out on solutions diluted 1:1 with pH 8 distilled water in order to match the concentration of nanoparticles, polysaccharides, and citrate administered with the complexed nanosystems.

Preparation of Complexes FeCi with Polysaccharides

Prior to complexation with polysaccharides, FeCi nanoparticles were sonicated in an ultrasonic bath for four cycles of 5 min interspersed with 1 min breaks (Bandelin Sonorex RK100 transistor, Berlin, Germany). FeCi nanoparticles were diluted 1:1 with APS or EPS stock solution and incubated overnight at 4 °C. This protocol was repeated concurrently with each administration throughout the experimentation time.

Both types of formulations studied in this work, i.e., FeCi + APS and FeCi + EPS, were stable for more than 1 month if kept at 4 °C in closed vessels. This stability over time was checked by DLS and ZP measurements, which ensured that the size of the aggregates and their surface charge did not vary by more than 10%.

https://doi.org/10.1021/acssuschemeng.6c01219
ACS Sustainable Chem. Eng. XXXX, XXX, XXX−XXX

Physicochemical Characterization and Morphological Analysis

DLS measurements were performed on a Zetasizer Nano ZS (ZEN 1600 model, Malvern Instruments, Southborough, MA), equipped with a He−Ne 633 nm, 4 mW laser and backscattering optics at a 173° detection angle. DLS analyses were performed over 11 runs in duplicate. The ZP analysis was carried out using a Zetasizer Pro Instrument (Malvern Panalytical Co., Ltd., Malvern, UK) using DTS1070 cells, maintained at 25 °C. Each reported ZP value was averaged over three runs. Transmission electron microscopy (TEM) measurements were conducted at CEME—Centro di Microscopie Elettroniche "Laura Bonzi", CNR Research Area (Florence, Italy). The instrument used for this purpose was a Gaia 3 (Tescan s.r.o., Brno, Czech Republic). A preliminary study of small-angle light scattering (SAXS) was carried out at the high-brilliance beamline ID02 of the European Synchrotron Radiation Facility (ESRF), Grenoble, France. The wavelength of the incident photons was $\lambda = 1$ Å. The range of the scattering vector q was 0.01−1 1/Å, with a sample−detector distance of 0.8 m. Samples were analyzed in a flow-through cell with a diameter of 2 mm and a temperature of 24 °C.

Application on *Tillandsia usneoides*

Three *T. usneoides* plants were bought at a local nursery (Giulio Celandroni Orchidee, San Giuliano Terme, Pisa) and maintained in a growth chamber set with the following parameters: 24/16 °C day/night, light intensity 300 μmol/m^{2}s, a 16-h (day) photoperiod, and relative humidity 60−65%. Three strands were taken for every treatment from each of the three plants, resulting in nine replicas per treatment. *T. usneoides* does not have absorbing roots and normally live suspended on tree branches. Also, its stem is very short and the leaves are the most visible part of the plant. For this reason, we could not measure the stem separately from the rest of the plant and we used the term "length" to indicate the total dimension of an individual, henceforth defined as "filament". All filaments were measured and selected according to two criteria: 1) weight and length of approximately 1 g and 30 cm, respectively, and 2) a number of ramifications not greater than five. Plants were hung upon ten plastic nets according to the type of treatment applied, and the strands were maintained in the growth chamber at a distance of 50 cm from each other, as depicted in Figure 1.

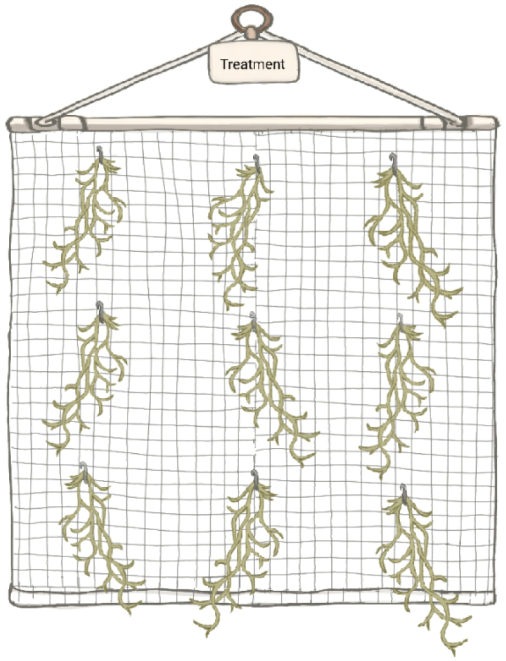

Figure 1. Scheme of strand disposition on the net.

Uniform light exposure was ensured by cyclically changing the filament position, while an adequate hydration level was guaranteed by spraying each strand with 3 mL of distilled water twice a week. Experiments on *T. usneoides* lasted for 31 days, during which 2 mL of the designed treatment was administered to each strand three times a week through foliar spray, in addition to collecting data on plant growth and fluorescence parameters. To administer the nanosystems, each net was removed from the growth chamber and placed in a box located in a separate room for spraying. Between treatments, the room was well ventilated to avoid airborne residual nanoparticles. The applied treatments with the respective concentration are presented in Table 1.

Plant Growth

Strand growth was monitored at each evaluated time by measuring their length using the software ImageJ 1.53t (Java 1.8.0_345 (64-bit); Rasband, W.S., ImageJ, U.S. National Institutes of Health, Bethesda, Maryland, USA, http://imagej.nih.gov/ij/). These measurements included all of the existing ramifications, thus obtaining the cumulative length for each strand.

Fluorescence Parameters

Chlorophyll fluorescence was evaluated using the portable fluorimeter Plant Efficiency Analyzer—Handy PEA (Hansatech Instruments Ltd.) on leaf samples adapted to darkness for 20 min and then flashed for 1 s with a saturated (1800 μmol m^{-2} s^{-1}) LED red light pulse (650 nm). During these measurements, two parameters were recorded: 1) the potential quantum efficiency of photosystem II Fv/Fm; 2) the general indicator of photosystem I and II efficiency Pindex (Performance index).

Element Determination

Plant samples were analyzed with monochromatic X-ray fluorescence analysis (E-max ULTRA, Z-Spec). The XRF analysis of the plant powdered material was performed using a Z-Spec E-max instrument (Z-Spec Inc.) in "Plant" mode.[47] This instrumentation uses monochromatic X-ray fluorescence excitation at 17.48 keV to analyze elements from Z = 13 (Al) to 40 (Zr) on the K-lines and up to 92 (U) on the L-lines. After collecting the strands at T31, the samples were placed in an oven set at 40 °C and left to dry for a week. For each treatment, three replicas were then individually pulverized with a mortar and pestle. Around 50 mg of the produced fine powder was covered with a thin film (12 μm) of polypropylene and measured for 60 s. Each sample was analyzed in three replicates by rotating the sample cup by 120 degrees: all the collected measurements were then averaged together. LGC7162—strawberry leaves were used as the certified reference material.

Statistics

The experiment comprised ten groups of plants, each with nine biological replicates. Plant length and chlorophyll fluorescence measurements were measured over time during the 31-day experimental period, at different time points: 7, 14, 21, 25, 28, and 31 days. Linear regression was used to analyze plant growth data (GraphPad Prism 7, GraphPad Software, San Diego, CA), with plant length increment as the dependent variable and the sampling time as independent one. The slope of the linear regression was considered as a descriptor of the plant growth rate.[48] Differences among means at the same experimental time points, as well as among the slope values, were assessed using one-way ANOVA ($p < 0.05$) in GraphPad Prism 7, followed by Tukey's HSD test for posthoc comparisons.

RESULTS AND DISCUSSION

Physicochemical Characterization

Table 1 shows the average diameter (obtained from the DLS intensity-weighted distribution) and the polydispersity index of bare and citrate-stabilized nanoparticles as well as of the polysaccharides alone and of the composite systems used in this study. The average size measured by DLS for FeN is much larger than what is extracted from TEM images on the same

https://doi.org/10.1021/acssuschemeng.6c01219
ACS Sustainable Chem. Eng. XXXX, XXX, XXX−XXX

Table 1. List of the Treatments Administered on *T. usneoides* with Their Respective Abbreviations and Concentrations

Treatment acronym	Type of treatment	[Fe] mg/mL	[Ci] mg/mL	[APS] mg/mL	[EPS] mg/mL
H_2O	pH8 distilled water				
FeN	Naked Fe_3O_4 nanoparticles	0.625			
FeCi	Citrated Fe_3O_4 nanoparticles	0.625	0.025		
Ci	Citrate		0.025		
APS	*A. vera* extract			1.25	
EPS	*C. capsulata* polysaccharides				1.25
Ci + APS	Citrate with *A. vera* extract		0.025	1.25	
Ci + EPS	Citrate with *C. capsulata* polysaccharides		0.025		1.25
FeCi + APS	Citrated Fe_3O_4 nanoparticles complexed with *A. vera* extract	0.625	0.025	1.25	
FeCi + EPS	Citrated Fe_3O_4 nanoparticles complexed with *C. capsulata* polysaccharides	0.625	0.025		1.25

system.[21] This clearly indicates that large transient aggregates were formed in solution when no stirring was applied, as expected for noncoated magnetic nanoparticles at such a pH. However, these aggregates could be easily resuspended and their presence did not prevent the administration of FeN to plants.

FeCi nanoparticles had a mean diameter of 33 ± 1 nm, showing that the FeN particles were capped by 1−2 layers of citrate ions, consistently with the good stability of this colloidal suspension (essentially provided by electrostatic interactions) in agreement with previous results.[49]

Concerning the polysaccharides, the diameter of APS aggregates ranged between 380 and 470, while for EPS, the measured diameter was much larger, reaching the limits of detectability in DLS experiments. We can explain this behavior by assuming that the chains of EPS do not assume a coil conformation in water, remaining stretched out in wires. This picture was confirmed by looking at the autocorrelation function (Figure 2), which presents an irregular, possibly not

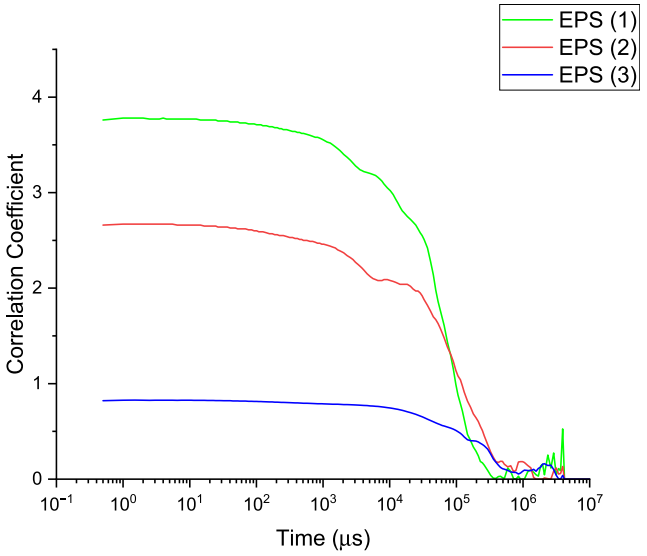

Figure 2. Autocorrelation functions of self-assembled EPS measured by a Zetasizer Pro instrument in three different runs.

monomodal, decay with an inflection at times much longer than the usual nano- or submicron size particles (see Figures S1−S5 in the SI for comparison with the other systems studied in this work). By contrast, the DLS measurements of FeCi formulations coated with APS and EPS showed the presence of well-defined scattering objects, ensuring that globular aggregates were formed by the interactions of FeCi nanoparticles and these two polysaccharides in solution. Specifically, only one population of aggregates was detected in the FeCi + APS systems, while in the FeCi + EPS a second contribution of about 1.5 μm in size (equivalent spherical diameter) was detected in small amount (≤10% of the total), which could be attributed to a minor fraction of noncomplexed polymer chains.

In line with this interpretation, the PDI FeCi + APS was 0.17, corresponding to low polydispersity, while for FeCi + EPS the PDI was higher, i.e., 0.5. Notwithstanding this evidence, which could suggest weak interaction of EPS with nanoparticles, their physicochemical affinity was unambiguously assessed by SAXS. Figure 3 shows the SAXS intensity

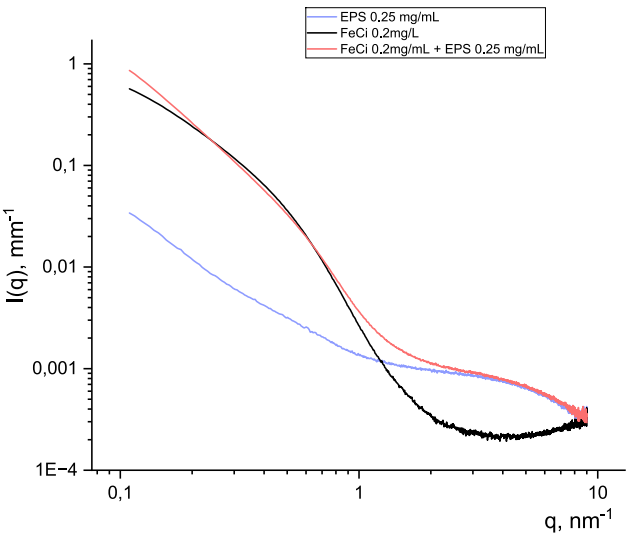

Figure 3. SAXS intensity diagrams of EPS, FeCi, and the complex FeCi + EPS.

diagrams of the EPS, FeCi, and FeCi + EPS samples. The curve of the polymer was a featureless decay typical of structurally ill-defined aggregates in solution, in agreement with the picture suggested by DLS. At low q, the scattering intensity of the systems containing nanoparticles was higher due to the electron density contrast of Fe_3O_4 with respect to organic molecules. At intermediate q the onset of a form factor in the SAXS diagram of FeCi + APS was clearly the signature of composite formation, while the shoulder at high q reported on a characteristic length associated with the morphology of the EPS chains.

https://doi.org/10.1021/acssuschemeng.6c01219
ACS Sustainable Chem. Eng. XXXX, XXX, XXX−XXX

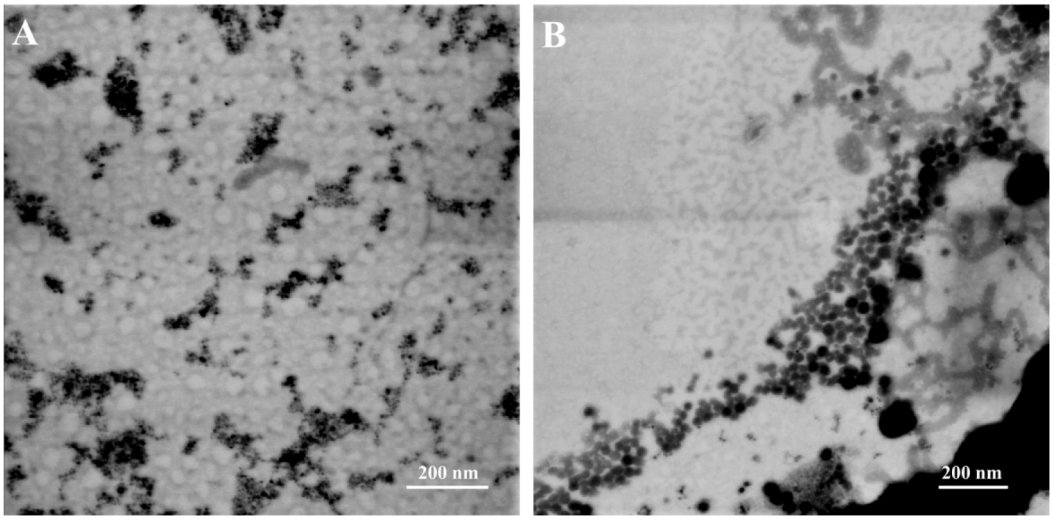

Figure 4. TEM micrographs of FeCi nanoparticles complexed with APS (A) and EPS (B). Mag: (A) 220kx; (B) 246kx.

DLS measurement showed that the average radius of both FeCi-polymer systems was compatible with the stomatal pore size (~5 to 7 μm[50]), while zeta potential (ZP) analysis evidenced a negative surface charge. The ZP values were in the range −20 to −35 mV, confirming the stability also observed during their application (see below).

TEM Micrographs

TEM images of bare iron oxide nanoparticles (FeN) and FeCi are shown in Figure S6A and B, respectively. Although TEM images are not fully representative of the colloidal state of nanoparticles in solution, we note that FeN formed larger agglomerates with sizes in the range of 1−2 μm, whereas FeCi were almost spherical and monodisperse, with diameters of 30−40 nm. This difference in morphology was consistent with their behavior in solution, as inferred by DLS, in that FeN underwent precipitation and coalescence, while FeCi remained stable in aqueous solution at pH 8.

Figure 4A and B shows TEM images of FeCi complexed with APS and EPS, respectively. As shown in Figure 4A, FeCi nanoparticles formed clusters with heterogeneous morphology embedded within a polymeric layer attributed to APS. These observations are consistent with the DLS analysis and indicate that the APS-nanoparticle complexes have slightly larger sizes with respect to the FeCi nanoparticles. Figure 4B shows that EPS partially covered the nanoparticle surface, leading to the formation of clusters in which the nanoparticles were entrapped. A significant fraction of the EPS polymer remained nonassociated with FeCi nanoparticles. This can be traced back to the smaller size population detected by DLS (Table 2).

As mentioned above, all of the nanoformulations studied in this work had a negative surface charge in water at pH = 8. The obtained ZP values are reported in Table 2. Citrate-stabilized nanoparticles gave higher absolute values than bare nanoparticles (−44 and −35 mV for FeCi and FeN, respectively), confirming the binding with citrate anions. This was surely the main reason for the enhanced stability of the citrate-capped magnetite nanoparticles. APS aggregates in solution showed a zeta potential of approximately −26 mV, while the FeCi−APS complexes had a zeta potential of −32 mV. EPS aggregates alone displayed a lower surface charge (−8 mV), and accordingly, the zeta potential of the FeCi + APS composite was closer to neutrality (−25 mV) than its APS counterpart.

Table 2. Average Diameter and Polydispersity Index of Bare Nanoparticles (FeN) Citrated Stabilized Nanosystems (FeCi), Polysaccharides Alone (APS and EPS), and the Complexes FeCi + APS and FeCi + EPS, Respectively, Obtained from DLS Intensity Weighted Distribution

Treatment acronym	Size average, nm	PDI	Zeta potential
FeN	600 ± 50	0.6	−35 ± 1
FeCi	33 ± 1	0.16	−44 ± 1
APS	420 ± 50	0.6	−26 ± 1
EPS	-	-	−8 ± 1
FeCi + APS	35 ± 1	0.17	−32 ± 1
FeCi + EPS	120 ± 40 (~90%) ≥1000 (10%)	0.5	−25 ± 1

We can speculate that the lower charge density (in absolute value) of EPS led to larger aggregates and that these latter were less efficient at covering the nanoparticle surfaces. Thus, the complexation behavior appears to be governed more by morphological constraints than by electrostatics. We can also suppose that EPS was less able to unfold or reorganize easily at the interface compared with APS, which could benefit from greater conformational flexibility due to the presence of smaller molecular components in the extract.

Effect on Plant Growth and Photosynthetic Parameters

At the end of the experiment, FeCi + APS treatment produced the highest increase in length (Figure 5), compared with the water-treated group and the other treatments, followed only by APS-alone exposure. The increase in length over time is reported in Table S1 and was used to calculate the slope of the regression line as a proxy of the growth rate. Notably, APS-treated specimens and, to a greater extent, FeCi + APS-treated plants exhibited the highest growth rates (respectively ~50% and 100% increase with respect to the control), while bare or citrate-capped nanoparticles did not affect growth (Figure 5B). Therefore, for the first time, these results demonstrate that the coating of nanoparticles can turn them from inefficient to efficient vectors of micronutrients provided that an appropriate material such as APS is used. Actually, *Aloe* vera leaf extract can contain numerous bioactive compounds, such as phytohormones, as analyzed by Alkuwayti et al. (2022)[30] that could explain the stimulatory effect shown by APS treatment alone.

https://doi.org/10.1021/acssuschemeng.6c01219
ACS Sustainable Chem. Eng. XXXX, XXX, XXX−XXX

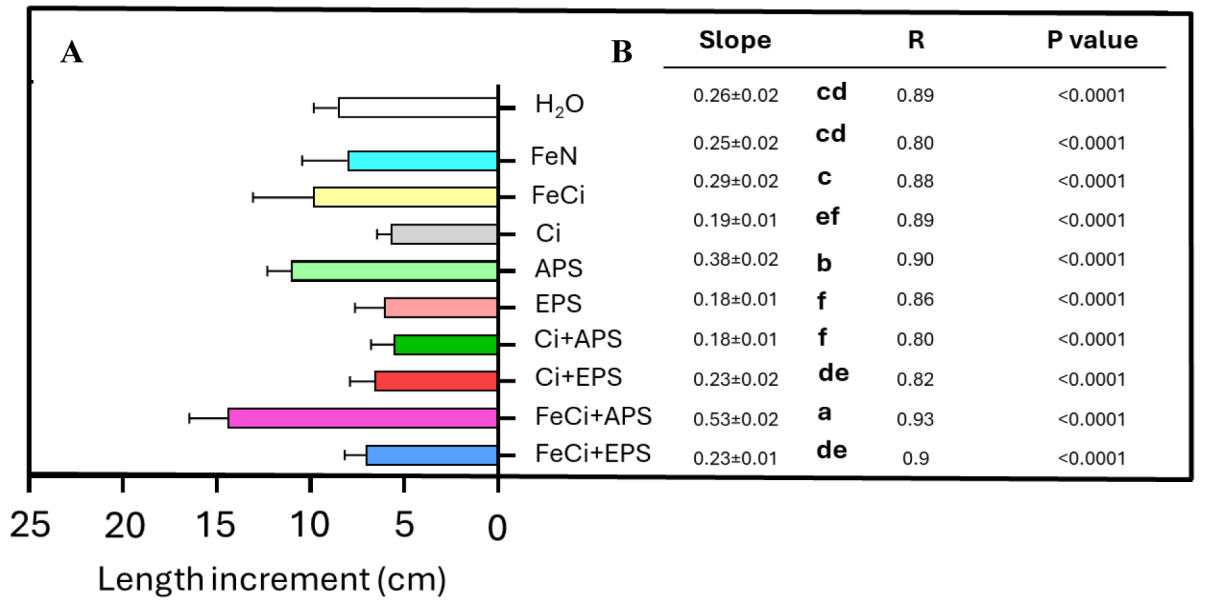

Figure 5. A) Final increment in length (cm) of *Tillandsia usneoides* strands exposed to the most relevant treatments indicated in Table 1 for 31 days. The increment was calculated by subtracting the length values at the beginning of the treatment to the values measured at the end of the treatment. Letters close to the histograms indicate significant differences among treatments, according to Tukey's test (at least $p < 0.01$). The reported values are means of 9 replicates + standard deviation. B) Growth rate of *T. usneoides* strands exposed to the treatments for 31 days calculated as the slope of the linear regression between plant length increment and sampling time.

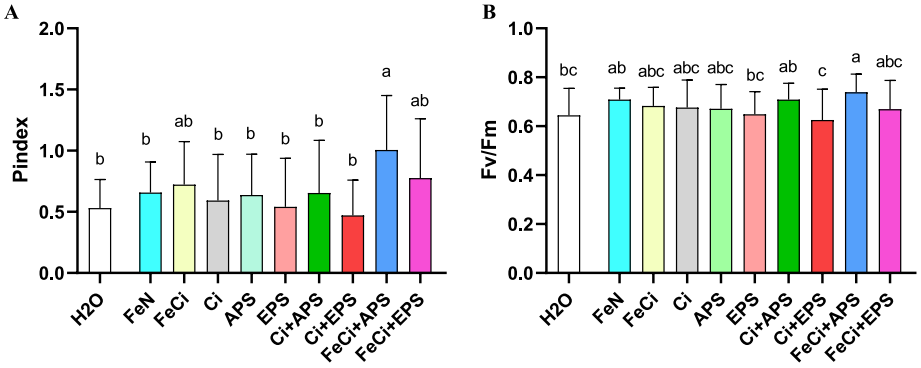

Figure 6. A) Pindex and B) Fv/Fm values of *Tillandsia usneoides* strands exposed to the most relevant treatments indicated in Table 1 for 31 days. The increment was calculated by subtracting the length values at the beginning of the treatment to the values measured at the end of the treatment. Letters close to the histograms indicate significant differences among treatments, according to Tukey's test (at least $p < 0.01$). The reported values are means of 9 replicates + standard deviation.

For example, growth-promoting effects have been demonstrated using foliar spray of *Aloe vera* leaf extract on dwarf umbrella tree (*Schefflera arboricola*).[51] In addition, other organic compounds contained in the Aloe extract, like organic acids and glucosides (as indicated on the label Aloe Detox Zero), could facilitate the acquisition of iron from nanoparticles, thus making the FeCi + APS the most effective in promoting plant growth.

Regarding the photosynthetic parameters, Pindex and Fv/Fm values in control and treated samples over the entire exposure period are reported in Tables S2 and S3, respectively. One-way ANOVA did not show any significant differences among the treatments at any time point, despite an increase in the values of both the indices observed in the FeCi + APS group toward the end of the experiment. At T31, plants treated with FeCi + APS showed the highest values of Pindex and Fv/Fm, which were significantly different from those of the control group (Figure 6A and B), thus explaining, at least in part, their enhanced growth through an ameliorated photosynthetic activity. No significant differences were observed in plants exposed to Ci, APS, or EPS treatment compared with the control.

Figure 7 reports the effect of different treatments on the iron concentration in washed and unwashed *T. usneoides* strands (the latter shown as bars with a diagonal line pattern). All the samples exposed to nanoparticles showed an increase in iron concentration compared with control and Ci + polysaccharides treatments, while the washing of the strands produced significantly lower iron levels only in plants treated with FeCi + EPS. On the contrary, when citrate and polysaccharides alone were applied iron accumulation did not display any variation. Apparently, the larger dimension (over 1000 nm) of most of the FeCi + EPS particles prevented their entry into the plants, as indicated by the dramatic lowering of Fe concentration measured after removing the particles loosely adhered to the plant surface by the washing procedure.

https://doi.org/10.1021/acssuschemeng.6c01219
ACS Sustainable Chem. Eng. XXXX, XXX, XXX−XXX

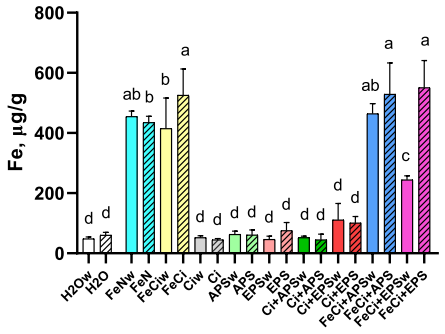

Figure 7. Iron amount (µg/g) in *Tillandsia usneoides* strands under different conditions, comparing washed samples ("w") with unwashed strands (bars with a diagonal line pattern).

Regarding the other treatments, the high iron concentration of the samples, combined to unchanged values after washing, suggested the internalization of particles inside the plants, possibly due to their lower dimension and more globular shape. Among the latter, once entered the plant, only FeCi + APS particles were able to induce growth.

The better performance of iron at the nanoscale with respect to bulk mineral salts could thus be ascribed to enhanced absorption and assimilation, facilitated transport in the vascular system and increased utilization by different organs.[52] In turn, the higher iron availability in the FeCi + APS samples could be the cause of the observed net higher photosynthetic performance, since this essential element is involved in chlorophyll biosynthesis and electron transport processes, thus explaining the enhanced growth.[53] The effects observed on growth and photosynthesis could be attributed exclusively to iron, since no significant differences were observed for the other elements (Ca, Cu, K, Mn, and Zn), as shown in Table S4.

CONCLUSION

The systems studied in this work constitute a novelty in the field of nanofertilizers. Due to the natural sources of the polysaccharides used, the resulting formulations show a rather complex composition and structure, which could be deciphered only by performing in-depth physicochemical characterization.

Experiments on *T. usneoides* evidenced an improvement of plant growth correlated to the administration of FeCi + APS and an increase of the photosynthetic activity, probably due to ameliorated iron nutrition. This effect was attributed to a synergistic interaction between the applied nanoparticles and the polysaccharides. The resulting improvement in plant growth opens the way to new agricultural applications that may contribute to alleviating hidden hunger, in line with the objectives of the ONU 2030 Agenda for Sustainable Development. In the future we aim to engineer these nanohybrids and scale up their production using flow chemistry and microreactors as a sustainable strategy.[54]

ASSOCIATED CONTENT

Supporting Information

The Supporting Information is available free of charge at https://pubs.acs.org/doi/10.1021/acssuschemeng.6c01219.

Additional experimental data on DLS, SEM images, length increments, photosynthetic parameters and element amount (PDF)

AUTHOR INFORMATION

Corresponding Author

Sara Falsini − *Department of Biology, University of Florence, Florence 50121, Italy;* orcid.org/0000-0003-2953-4025; Email: sara.falsini@unifi.it

Authors

Veronica Butelli − *Department of Biology, University of Florence, Florence 50121, Italy*

Alessio Papini − *Department of Biology, University of Florence, Florence 50121, Italy*

Maria Cristina Salvatici − *Centro di Microscopie Elettroniche "Laura Bonzi", ICCOM, National Research Council (CNR), Sesto Fiorentino, FI 50019, Italy*

Delphine Talbot − *PHysicochimie des Électrolytes et Nanosystèmes InterfaciauX (PHENIX), Sorbonne Université, CNRS, Paris 75005, France*

Ali Abou-Hassan − *PHysicochimie des Électrolytes et Nanosystèmes InterfaciauX (PHENIX), Sorbonne Université, CNRS, Paris 75005, France; Institut Universitaire de France (IUF), Paris 75231, France;* orcid.org/0000-0002-9070-1024

Cristina Gonnelli − *Department of Biology, University of Florence, Florence 50121, Italy;* orcid.org/0000-0001-5201-586X

Sandra Ristori − *Department of Chemistry "Ugo Schiff" &CSGI, University of Florence, Sesto Fiorentino, FI 50019, Italy;* orcid.org/0000-0003-0708-3956

Complete contact information is available at: https://pubs.acs.org/10.1021/acssuschemeng.6c01219

Notes

The authors declare no competing financial interest.

ACKNOWLEDGMENTS

We thank Emma Chiani, a bachelor's degree student, for her valuable contribution to this work. We acknowledge the European Synchrotron Radiation Facility (ESRF) for beamtime provision. In particular, we would like to thank Dr. Theyencheri Narayanan and Dr. Michael Szutcki for their assistance and support in using the ID02 beamline. We thank the Partnership for Soft Condensed Matter (PSCM) for the use of DLS and PZ to check the samples' stability before and after SAXS experiments. We also acknowledge the project, Plantform no. F/310143/01-03/X56, "Accordo per l'innovazione 18/10/2023", Ministry of Enterprise and Made in Italy for financial support. This manuscript reflects only the authors' views and opinions, neither the European Union nor the European Commission can be considered responsible for them.

REFERENCES

(1) Buriak, J. M.; Liz-Marzán, L. M.; Parak, W. J.; Chen, X. Nano and Plants. *ACS Nano* **2022**, *16*, 1681−1684.

(2) Zezzi Arruda, M. A.; Santos da Silva, A. B.; Seiko Kato, L. There Is Plenty of Room in Plant Science: Nanobiotechnology as an Emerging Area Applied to Somatic Embryogenesis. *J. Agric. Food Chem.* **2023**, *71*, 3651−3657.

(3) Meng, Y.; Feng, Y.; Bai, X.; Yu, Q.; Zhou, J.; Wang, J. Application of Nanotechnology in Agricultural Sustainability: Absorption, Translocation, and Challenges of Nanoparticles. *Curr. Plant Biol.* **2025**, *42*, 100492.

(4) Clemente, I.; Falsini, S.; Di Cola, E.; Fadda, G. C.; Gonnelli, C.; Spinozzi, F.; Bacia-Verloop, M.; Grillo, I.; Ristori, S. Green Nanovectors for Phytodrug Delivery: In-Depth Structural and Morphological Characterization. *ACS Sustainable Chem. Eng.* **2019**, *7*, 12838−12846.
(5) Safdar, M.; Kim, W.; Park, S.; Gwon, Y.; Kim, Y.-O.; Kim, J. Engineering Plants with Carbon Nanotubes: A Sustainable Agriculture Approach. *J. Nanobiotechnol.* **2022**, *20*, 275.
(6) Falsini, S.; Rosi, M. C.; Urciuoli, S.; Andreani, A.; Papini, A.; Gonnelli, C.; Ristori, S. Nanoformulations from Olive Pomace to Enhance the Efficacy of Hydroxytyrosol as a Natural Pest Control Agent. *Environ. Sci.: Nano* **2024**, *11*, 3625−3636.
(7) Gaglio, S. C.; Zanella, G.; Cazzaniga, S.; Olivieri, N.; Battagini, E.; Romeo, A.; Ballottari, M.; Perduca, M. Enhanced Stability and Photochemical Activity of Photosystem I from the Green Alga *Chlamydomonas reinhardtii* upon Encapsulation in Organic Matrixes. *ACS Sustainable Chem. Eng.* **2025**, *13*, 5046−5056.
(8) Kempken, F.; Jung, C. *Genetic Modification of Plants*; Springer: Heidelberg, 2010. DOI: .
(9) Abdul Aziz, M.; Brini, F.; Rouached, H.; Masmoudi, K. Genetically Engineered Crops for Sustainably Enhanced Food Production Systems. *Front. Plant Sci.* **2022**, *13*, 1027828.
(10) Das, J. K.; Padhani, Z. A. Alleviating Hidden Hunger: An Infallible Bridge to Improved Health and Nutrition. *Lancet Glob. Health* **2022**, *10* (11), No. e1539−e1540.
(11) Fageria, N. K.; Baligar, V. C.; Clark, R. B. Micronutrients in Crop Production. In *Advances in Agronomy*; Sparks, D. L., ed.; Academic Press, 2002, Vol. *77*, pp. 185−268. DOI: .
(12) *Plant Micronutrients: deficiency and Toxicity Management*, Aftab, T.; Rehman Hakeem, K., Eds.; Springer, 2020.
(13) Chorianopoulou, S. N.; Bouranis, D. L. The Role of Sulfur in Agronomic Biofortification with Essential Micronutrients. *Plants* **2022**, *11* (15), 1979.
(14) Khan, M.; Ali, N.; Rafi, M.; Vimal, A.; Vishvakarma, R. Nanofertilizers: Revolutionizing Nutrient Delivery in Crops. In *Handbook of Nanotechnology in Agriculture*, Husen, A.; Springer, 2025.
(15) Schönherr, J. Characterization of Aqueous Pores in Plant Cuticles and Permeation of Ionic Solutes. *J. Exp. Bot.* **2006**, *57* (11), 2471−2491.
(16) Haddad, M.; Nassar, D.; Shtaya, M. Heavy metals accumulation in soil and uptake by barley (*Hordeum vulgare*) irrigated with contaminated water. *Sci. Rep.* **2023**, *13* (1), 4121.
(17) Qiao, S.; Bu, X.; Zhou, Y.; Yang, Y.; Yang, X.; Yang, J. Nanoparticles in Agricultural Soil. *J. Agric. Food Chem.* **2026**, *74* (2), 1891−1910.
(18) Dance, A. Plants Have a Secret Language that Scientists Are Only Now Starting to Decipher. *Nature* **2025**, *646*, 1044−1046.
(19) Ma, C.; White, J. C.; Dhankher, O. M.; Xing, B. Metal-Based Nanotoxicity and Detoxification Pathways in Higher Plants. *Env. Sci. Technol.* **2015**, *49*, 7109.
(20) Rastogi, A.; Zivcak, M.; Sytar, O.; Kalaji, H. M.; He, X.; Mbarki, S.; Brestic, M. Impact of Metal and Metal Oxide Nanoparticles on Plant: A Critical Review. *Front. Chem.* **2017**, *5*, 78.
(21) Falsini, S.; Colzi, I.; Dainelli, M.; Parigi, E.; Salvatici, M. C.; Papini, A.; Talbot, D.; Abou-Hassan, A.; Gonnelli, C.; Ristori, S. Impact of airborne iron oxide nanoparticles on *Tillandsia usneoides* as a model plant to assess pollution in heavy traffic areas. *Chemosphere* **2024**, *355*, 141765.
(22) Van de Walle, A.; Figuerola, A.; Espinosa, A.; Abou-Hassan, A.; Estrader, M.; Wilhelm, C. Emergence of Magnetic Nanoparticles in Photothermal and Ferroptotic Therapies. *Mater. Horiz.* **2023**, *10*, 4757−4775.
(23) Cabana, S.; Curcio, A.; Michel, A.; Wilhelm, C.; Abou-Hassan, A. Iron Oxide Mediated Photothermal Therapy in the Second Biological Window: A Comparative Study between Magnetite/Maghemite Nanospheres and Nanoflowers. *Nanomaterials* **2020**, *10*, 1548.
(24) Miron, C. E.; Petitjean, A. Sugar Recognition: Designing Artificial Receptors for Applications in Biological Diagnostics and Imaging. *ChemBioChem* **2015**, *16* (3), 365−379.
(25) Tommasone, S.; Allabush, F.; Tagger, Y. K.; Norman, J.; Köpf, M.; Tucker, J. H. R.; Mendes, P. M. The Challenges of Glycan Recognition with Natural and Artificial Receptors. *Chem. Soc. Rev.* **2019**, *48* (22), 5488−5505.
(26) Shogren, R.; Wood, D.; Orts, W.; Glenn, G. Plant-Based Materials and Transitioning to a Circular Economy. *Sustainable Prod. Consum.* **2019**, *19*, 194−215.
(27) Chong, P. L.; Singh, A. K.; Kok, S. L. Potential Application of *Aloe vera*−Derived Plant-Based Cell in Powering Wireless Device for Remote Sensor Activation. *PLoS One* **2019**, *14*, No. e0227153.
(28) Comas-Serra, F.; Miró, J. L.; Umaña, M. M.; Minjares-Fuentes, R.; Femenia, A.; Mota-Ituarte, M.; Pedroza-Sandoval, A. Role of Acemannan and Pectic Polysaccharides in Saline-Water Stress Tolerance of *Aloe vera* (*Aloe barbadensis Miller*) Plant. *Int. J. Biol. Macromol.* **2024**, *268*, 131601.
(29) Sharma, P.; Kaur, R. A Comprehensive Review of Aloe vera: Composition, Properties, Processing, and Applications. *Nat. Prod. J.* **2026**, *16*, 15.
(30) Alkuwayti, M. A.; Aldayel, M. F.; Yap, Y.-K.; El Sherif, F. Exogenous Application of Aloe vera Leaf Extract Improves Silybin Content in *Silybum marianum* L. by Up-Regulating Chalcone Synthase Gene. *Agriculture* **2022**, *12*, 1649.
(31) Abbas, S.; Zaglool, M.; El-Ghadban, E.; El-Kareem, S. A.; Waly, A. Effect of Foliar Application with Aloe Leaf Extract (ALE) on Vegetative Growth, Oil Percentage, and Anatomical Leaf Structure of Sage (*Salvia officinalis* L.) Plant under Sand Soil Conditions. *Hortsci. J. Suez Canal. Univ.* **2016**, *5*, 9−14.
(32) El-Sherif, F. *Aloe vera* Leaf Extract as a Potential Growth Enhancer for *Populus* Trees Grown under *In Vitro* Conditions. *Am. J. Plant Biol.* **2017**, *2*, 101−105.
(33) Godlewska, K.; Biesiada, A.; Michalak, I.; Pacyga, P. The Effect of Botanical Extracts Obtained through Ultrasound-Assisted Extraction on White Head Cabbage (*Brassica oleracea* L. var*capitata* L.) Seedlings Grown under Controlled Conditions. *Sustainability* **2020**, *12*, 1871.
(34) Ei, E.; Park, H. H.; Kuk, Y. I. Growth Promotion and Secondary Metabolites of Vegetables by Spraying Soil with *Psidium guajava, Aloe vera*, *Allium sativum,* and *Medicago sativa* Extracts at Various Stages of Growth. *Plants* **2025**, *14*, 237.
(35) Sili, C.; Pelosi, E.; Vincenzini, M.; Materassi, R.; Florenzano, G. *Proceedings of the European Congress of Biotechnology*; 1984; Vol. *1*, pp 91−96.
(36) Florenzano, G.; Sili, C.; Pelosi, E.; Vincenzini, M. Cyanospira rippkae and *Cyanospira capsulata* (gen. nov. and spp. nov.): New Filamentous Heterocystous Cyanobacteria from Magadi Lake (Kenya). *Arch. Microbiol.* **1985**, *140*, 301−306.
(37) Garozzo, D.; Impallomeni, G.; Spina, E.; Sturiale, L. The Structure of the Exocellular Polysaccharide from the Cyanobacterium *Cyanospira capsulata*. *Carbohydr. Res.* **1998**, *307*, 113−124.
(38) De Philippis, R.; Sili, C.; Vincenzini, M.; Materassi, R. *Recent Developments in Industrial Polysaccharides*; Crescenzi, V.; Dea, I. C. M.; Paoletti, S.; Sutherland, I. W.; Gordon & Breach: NY, 1989; p 203.
(39) Braun, J. C. A.; Colla, L. M. Use of Microalgae for the Development of Biofertilizers and Biostimulants. *BioEnergy Res.* **2023**, *16*, 289−310.
(40) Guardiola-Márquez, C. E.; Martínez-Ballesta, M. D. C.; García-Sánchez, C. V.; Bojorquez-Rodríguez, E. M.; Jacobo-Velázquez, D. A.; Martínez-Hernández, G. B. Effects of Foliar and Root Application of Zn and Fe Bio-Nanofertilizers on the Glucosinolate, Zn, and Fe Contents of Pak Choi (*Brassica rapa* subsp. chinensis) Grown under Hydroponic and Pot Cultivation. *Sci. Hortic.* **2024**, *338*, 113654.
(41) Brighigna, L.; Papini, A.; Mosti, S.; Cornia, A.; Bocchini, P.; Galletti, G. The Use of Tropical Bromeliads (Tillandsia spp.) for Monitoring Atmospheric Pollution in the Town of Florence, Italy. *Rev. Biol. Trop.* **2002**, *50* (2), 577−584.

https://doi.org/10.1021/acssuschemeng.6c01219
ACS Sustainable Chem. Eng. XXXX, XXX, XXX−XXX

(42) Li, P.; Pemberton, R.; Zheng, G. Foliar Trichome-Aided Formaldehyde Uptake in the Epiphytic *Tillandsia velutina* and Its Response to Formaldehyde Pollution. *Chemosphere* **2015**, *119*, 662−667.
(43) Mosti, S.; Papini, A.; Brighigna, L. A New Quantitative Classification of Ecological Types in the Bromeliad Genus Tillandsia (Bromeliaceae) Based on Trichomes. *Rev. Biol. Trop.* **2008**, *56* (1), 191−203.
(44) Papini, A.; Tani, G.; Di Falco, P.; Brighigna, L. The Ultrastructure of the Development of Tillandsia (Bromeliaceae) Trichome. *Flora* **2010**, *205* (2), 94−100.
(45) Magiera, T.; Jablonska, M.; Strzyszcz, Z.; Rachwal, M. Morphological and mineralogical forms of technogenic magnetic particles in industrial dusts. *Atmos. Environ.* **2011**, *45* (25), 4281−4290.
(46) Vincenzini, M.; De Philippis, R.; Sili, C.; Materassi, R. Studies on exopolysaccharide release by diazotrophic batch cultures of Cyanospira capsulata. *Appl. Microbiol. Biotechnol.* **1990**, *34*, 392−396.
(47) Zhang, C.; Charrois, L.; Jacquet, J.; Sirguey, C.; Chen, Z.; van der Ent, A. Monochromatic X-ray fluorescence spectroscopy for major and trace element analysis in plant science applications. *Plant Soil* **2026**, *518*, 105−120.
(48) Falsini, S.; Colzi, I.; Chelazzi, D.; Dainelli, M.; Schiff, S.; Papini, A.; Coppi, A.; Gonnelli, C.; Ristori, S. Plastic is in the air: impact of micro-nanoplastics from airborne pollution on *Tillandsia usneoides* (L.) L. Bromeliaceae) as a possible green sensor. *J. Hazard. Mater.* **2022**, *437*, 129314.
(49) Martens, U.; Böttcher, D.; Talbot, D.; Bornscheuer, U.; Abou-Hassan, A.; Delcea, M. Maghemite nanoparticles stabilize the protein corona formed with transferrin presenting different iron-saturation levels. *Nanoscale* **2019**, *11*, 16063−16070.
(50) Martin, C. E.; Peters, E. A. Functional stomata of the atmospheric epiphyte *Tillandsia usneoides* L. *Bot. Gaz.* **1984**, *145* (4), 502−507.
(51) Hanafy, M. S.; Saadawy, F. M.; Milad, S. M. N.; Ali, R. M. Effect of some natural extracts on growth and chemical constituents of *Schefflera arboricola* plants. *J. Hortic. Sci. Ornam. Plants* **2012**, *4*, 26−33.
(52) De La Torre-Roche, R.; Cantu, J.; Tamez, C.; Zuverza-Mena, N.; Hamdi, H.; Adisa, I. O.; Elmer, W.; Gardea-Torresdey, J.; White, J. C. Seed biofortification by engineered nanomaterials: a pathway to alleviate malnutrition? *J. Agric. Food Chem.* **2020**, *68*, 12189−12202.
(53) Terry, N.; Low, G. Leaf chlorophyll content and its relation to the intracellular localization of iron. *J. Plant Nutr.* **1982**, *5* (4−7), 301−310.
(54) Falsini, S.; Bardi, U.; Abou- Hassan, A.; Ristori, S. Sustainable strategies for large-scale nanotechnology manufacturing for biomedical purposes. *Green Chem.* **2018**, *20*, 3897−3907.

https://doi.org/10.1021/acssuschemeng.6c01219
ACS Sustainable Chem. Eng. XXXX, XXX, XXX−XXX